Anions as Dynamic Probes for Ionic Liquid Mixtures

Maria Enrica Di Pietro,[a] Franca Castiglione,[a] and Andrea Mele.*[a,b]*

[a] Department of Chemistry, Materials and Chemical Engineering "G. Natta", Politecnico di Milano, Piazza L. da Vinci 32, 20133 Milano, Italy.

[b] CNR-ICRM Istituto di Chimica del Riconoscimento Molecolare, "U.O.S. Milano Politecnico", Via L. Mancinelli 7, 20131 Milano, Italy.

KEYWORDS. Room-temperature ionic liquids (RTILs); designer solvents; double salt ionic liquids (DSIL); diffusion NMR; relaxation NMR.

ABSTRACT. Ionic liquid (IL) mixtures have been proposed as a viable alternative to rationally fine-tune the physicochemical properties of ILs for a variety of applications. The understanding of the effects of mixing ILs on the properties of the mixtures is however only in the very early stages. Two series of ionic liquid mixtures, based on the 1-ethyl-3-methylimidazolium and 1-dodecyl-3-methylimidazolium cations, and having a common anion (tetrafluoroborate or bis(trifluoromethylsulfonyl)imide), have been prepared and deeply characterized *via* multiple NMR techniques. Diffusion and relaxation methods combined with 2D ion-ion correlation

(NOE) experiments have been used for a better understanding of the interplay between dynamics and structure of IL mixtures. A crucial role of the anion in driving the mixture's behaviour emerged, making them important "dynamic probes" for gaining information of the polar and non-polar regions of ionic liquids and their mixtures.

Introduction

Ionic liquids (ILs) are liquid materials that consist entirely of ions and usually melt below 100°C.[1,2] ILs have potentially a number of advantages, including very low vapour pressure, low flammability, high electrochemical stability, large liquid ranges and generally good thermal stability.[3] This has drawn considerable interest both among the academic community and in terms of industrial applications.[2,4–6]

A peculiar feature of ILs is the opportunity to fine-tune their properties for a given application by mixing and matching the cationic and anionic constituents and by altering and functionalizing the structure of the anion, cation, or both.[1] This has led to large libraries of ILs synthesised with the aim of achieving specific properties.[3] Next to the amount of synthetic work needed, this approach is hindered by the lack of toxicological characterization of the new ILs, which slows down, if not prevent, their industrial application. An alternative approach to increase such synthetic variety is to mix two, or more, toxicologically well-characterized ILs together to produce a range of new systems possessing combination of properties.[1,7–9]

Mixtures of ILs containing different cation and anion only started receiving significant attention in the last 10 to 15 years.[1,3,7,9–33] For a rational fine-tuning of the properties of IL

mixtures, the understanding of structural organization, motion and intermolecular interactions at the molecular level is pivotal to tailor the system for a given application.[24,29]

Here we focus on the structure and dynamics of mixtures based on 1-alkyl-3-methylimidazolium salts ([$C_n$mim][X]) with a common anion. We adopt the nomenclature based upon the number of components (instead of the number of constituents), hence we refer to the mixtures as binary mixtures.[1,8] Keeping the anion constant, two cations with a short chain $[C_2mim]^+$ and a long chain $[C_{12}mim]^+$ were chosen, as representatives of quite different dynamic and structural behaviours. The choice is intended to maximise the "anomalies" of the mixtures by combining an IL with no nanostructure, [C_2mim][X], with one containing the amphiphilic cation, $[C_{12}mim]^+$. Indeed, the available literature seems to converge upon the conclusion that most IL mixtures display close to ideal mixing behaviour and deviations may for instance occur in case of substantial differences in the ion sizes, as in the present study.[18,24,28,30] To gather detailed information on the modulation of the properties of the mixture, various molar ratios of the two components were studied, ranging from compositions with a marked excess of one component to equimolar mixtures. As for the anion, we selected two fluorinated species, bistriflimide, $[TFSI]^-$ (systematically known as bis(trifluoromethane)sulfonimide and often referred to as $[NTf_2]^-$), and tetrafluoroborate $[BF_4]^-$.

To the best of our knowledge, no investigation has been carried out on such mixtures in terms of dynamics. On the contrary, accurate recent studies reported on the (nano)structure of [C_2mim][C_{12}mim][TFSI] mixtures investigated by small-angle X-ray and neutron scattering measurements, as well as molecular dynamics (MD) simulations.[3,24] At low concentrations of [C_{12}mim][TFSI], isolated pseudospherical aggregates of $[C_{12}mim]^+$ were found within the polar network composed of the charged imidazolium heads and the $[TFSI]^-$ ions. The number of these

aggregates grows with increasing $[C_{12}mim][TFSI]$ concentration and coalesce to form a continuous, non-polar sub-phase. At high concentrations of $[C_{12}mim][TFSI]$, the liquid structure is similar to that of pure $[C_{12}mim][TFSI]$ and the system can be described as a bicontinuous network of continuous polar and nonpolar domains. Very recently also binary mixtures $[C_2mim]_x[C_8mim]_{1-x}[BF_4]$ were investigated by X-ray scattering and MD simulations.[14] Similarly to what found for $[C_2mim][C_{12}mim][TFSI]$ mixtures, a disruption of the bicontinuous morphology and a transition to more isolated aggregates upon dilution with $[C_2mim][BF_4]$ was observed. Analogous structural behaviours characterize also $[C_2mim][C_6mim][TFSI]$ and $[C_2mim][C_{10}mim][TFSI]$ mixtures, where the ethyl groups of $[C_2mim]^+$ turn out not to enter into the non-polar domains formed by the hexyl or decyl groups.[22,28] Contrarily, when two cations are combined with chains of more similar size, as in $[C_6mim][C_{10}mim]Cl$ and $[C_4mim][C_{10}mim][TFSI]$ mixtures, there is no differentiation between domains built up only by the short (butyl or hexyl) and the long (decyl) chains.[28,34] The different behaviour of such mixtures has been explained by assuming that the ethyl chains cannot enter into van der Waals dispersion interactions sufficiently to overcome those between the hexyl, decyl or dodecyl chains, hence the separation is maintained. On the other hand, the hexyl and decyl chains of $[C_6mim][C_{10}mim]Cl$ and the butyl and decyl chains of $[C_4mim][C_{10}mim][TFSI]$ can both enter into van der Waals dispersion interactions allowing their intimate mixing.

The focus of the previous studies is mainly the cation-cation mutual arrangement. From our viewpoint, what deserves now a closer look is the role played by the anion in the dynamic behaviour and structural organization of such mixtures. To shed light on this aspect, we selected two anions which are known to interact with a different strength to the imidazolium head of $[C_nmim]^+$ cations: a soft anion, $[TFSI]^-$, and a relatively hard one, $[BF_4]^-$.[35] Indeed, from

electrospray ionization mass spectrometry (ESI-MS) data it was possible to measure the relative strength of anion-cation interaction inside different ILs differentiating between two classes: anions tightly coordinated to the cationic moiety, that include $[BF_4]^-$, and anions loosely interacting with the alkylimidazolium species, such as $[TFSI]^-$.[35] Although pure TFSI-based ILs are known to be in general less structured materials than the analogous BF_4-based ILs, the effect of the anion on dynamics and structure of $[C_{12}mim][C_2mim][X]$ mixtures is still an unexplored issue.

The aim of the present work is then to contribute to filling the knowledge gap on IL mixtures in terms of dynamics and to widening the understanding of their nanostructure at the molecular level, with a special focus on the role of the anion.

To these end, multiple Nuclear Magnetic Resonance (NMR) techniques are applied. NMR stands out as a competitive and well-established method to get insights into structural and dynamic properties of ILs at the molecular level.[36,37] We present in the following a comprehensive NMR study of $[C_{12}mim][C_2mim][BF_4]$ and $[C_{12}mim][C_2mim][TFSI]$ mixtures. Spin-lattice and spin-spin NMR relaxation and pulsed field gradient spin-echo NMR are applied to gather information on the rotational and translational motion of the individual cations and anions in the mixture, while homo- and heteronuclear NOE correlations make it possible to detect the intermolecular interactions that are descriptors of the local structure of the mixtures.

Experimental Methods

Samples

The ionic liquids 1-ethyl-3-methylimidazolium tetrafluoroborate (99%), 1-ethyl-3-methylimidazolium bis(trifluoromethylsulfonyl)imide (99.5%), 1-dodecyl-3-methylimidazolium

tetrafluoroborate (>98%), 1-dodecyl-3-methylimidazolium bis(trifluoromethylsulfonyl)imide (98%) were purchased from Iolitec. The chemical structures of all cations and anions are depicted in Figure 1. Mixtures were prepared by mixing the pure components in the appropriate proportions. The six binary mixture series investigated in this work are listed in Table 1, together with the four pure components. They all display the general formula $[C_{12}mim]_{1-x}[C_2mim]_x[TFSI]$ and $[C_{12}mim]_{1-x}[C_2mim]_x[BF_4]$, with x = 0.1, 0.5, 0.9. Corresponding short names are also indicated, which will be used in the following for the sake of simplicity. After proper stirring, samples were dried under *vacuum* and transferred in 5 mm NMR tubes. The tubes, equipped with a capillary containing DMSO-d_6, were immediately flame-sealed after transferring the samples. While the water concentrations were not explicitly measured in the samples, the absence of a detectable water signal in the NMR spectra indicated that the water content is negligible.[38]

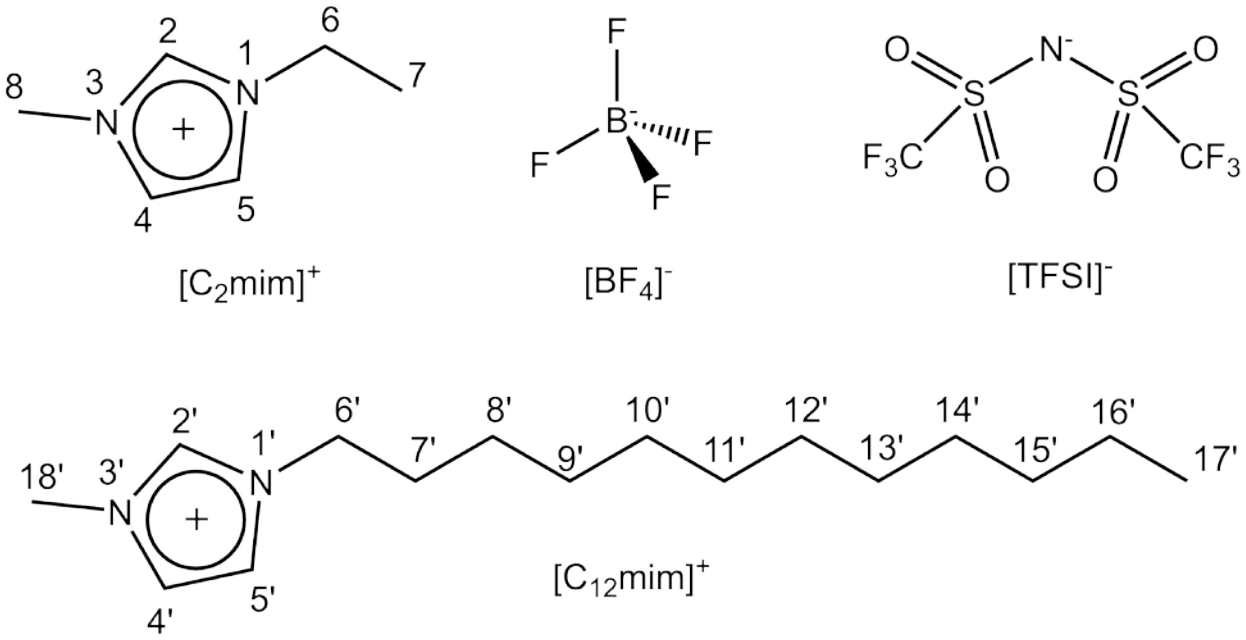

Figure 1. Structure and numbering of the cations and anions constituting the ionic liquids used in this work.

Table 1. Samples used in this work.

Short name	Description
BF_4-10:0	$[C_{12}mim][BF_4]$
BF_4-9:1	$[C_{12}mim]_{0.9}[C_2mim]_{0.1}[BF_4]$
BF_4-5:5	$[C_{12}mim]_{0.5}[C_2mim]_{0.5}[BF_4]$
BF_4-1:9	$[C_{12}mim]_{0.1}[C_2mim]_{0.9}[BF_4]$
BF_4-0:10	$[C_2mim][BF_4]$
TFSI-10:0	$[C_{12}mim][TFSI]$
TFSI-9:1	$[C_{12}mim]_{0.9}[C_2mim]_{0.1}[TFSI]$
TFSI-5:5	$[C_{12}mim]_{0.5}[C_2mim]_{0.5}[TFSI]$
TFSI-1:9	$[C_{12}mim]_{0.1}[C_2mim]_{0.9}[TFSI]$
TFSI-0:10	$[C_2mim][TFSI]$

NMR methods

^1H and ^{19}F NMR experiments were carried out on a Bruker Avance 500 spectrometer equipped with a 5 mm pulsed-field z-gradient QNP four nuclei switchable probe. HOESY experiments were carried out on a Bruker NEO 500 spectrometer equipped with a 5 mm pulsed-field z-gradient BBFO probe. For each sample, the probe was carefully tuned, and the 90° pulses evaluated. The sample temperature was set and controlled using a variable temperature control unit using air gas flow. Variable temperature experiments were performed changing the temperature from 300 K to 325 K.

T_1 and T_2 relaxation measurements were performed with the inversion recovery (IR) and the Carr-Purcell Meiboom-Gill (CPMG) pulse sequences, respectively. All relaxation measurements

were carried out with relaxation delays at least five times T_1. Cation and anion relaxation times were measured independently by carrying out IR and CPMG experiments in the ^{1}H and ^{19}F frequency domains, respectively.

The spin-lattice relaxation rates were measured using data matrices of 8192 (t_2) x 16 (t_1) and 32768 (t_2) x 16 (t_1) complex data points for ^{1}H and ^{19}F, respectively. Proton T_1 experiments were carried out over a spectral width of 14 ppm for various delay time τ, ranging from 0.01-5 s to 0.05-20 s (for BF_4-samples) and from 0.05-7 s to 0.05-40 s (for TFSI-samples), according to the temperature and molar composition of the sample. Fluorine T_1 experiments were carried out over a spectral width of 80 ppm for various delay time τ, ranging from 0.05-10 s to 0.05-20 s (for BF_4-samples) and from 0.05-10 s to 0.05-40 s (for TFSI-samples), according to the temperature and molar composition of the sample. A total of 8 transients per increments were collected for each T_1 experiment for both ^{1}H and ^{19}F.

The spin-spin relaxation rates were measured using data matrices of 8192 (t_2) x 16 (t_1) and 32768 (t_2) x 16 (t_1) complex data points for ^{1}H and ^{19}F, respectively. Proton T_2 experiments were carried out over a spectral width of 14 ppm for various echo time τ, ranging from 0.008-2 s to 0.02-10 s (for BF_4-samples) and from 0.008-2 s to 0.02-15 s (for TFSI-samples), according to the temperature and molar composition of the sample. Fluorine T_2 experiments were carried out over a spectral width of 80 ppm for various echo time τ, ranging from 0.008-2 s to 0.04-10 s (for BF_4-samples) and from 0.02-5 s to 0.04-20 s (for TFSI-samples), according to the temperature and molar composition of the sample. A total of 8 transients per increments were collected for each experiment T_2 for both ^{1}H and ^{19}F.

The baselines of all arrayed T_1 and T_2 spectra were corrected prior to processing the data. Data were processed using an exponential filter in F_2 dimension (with LB equal to 2 Hz for ^{1}H and 0.5

Hz for ^{19}F) and integrals were used in calculating relaxation times. Relaxation times were computed from experimental raw data by using the Bruker T_1/T_2 relaxation module with the standard one-component fitting function. Data were processed three times and errors were calculated from the maximum standard deviation found for the worst sample at the lowest temperature. Maximum errors are estimated to be 1% for T_1 and 5% for T_2.

Self-diffusion coefficients were measured by pulse gradient spin echo (PGSE) experiments by applying sine shaped pulsed magnetic field gradients along the z-direction up to a maximum strength of G = 53.5 G cm^{-1}. All the diffusion experiments were performed using the bipolar pulse longitudinal eddy current delay (BPP-LED) pulse sequence. Cation and anion self-diffusion coefficients were measured independently by carrying out PGSE experiments in the ^1H and ^{19}F frequency domains, respectively. All experiments were carried out over a spectral width of 14 ppm or 80 ppm for ^1H and ^{19}F, respectively, with a total of 8 transients per increments. The relaxation delay was set to at least five times T_1 and 8 dummy scans were programmed prior to acquisition. The pulse gradients were incremented from 2 to 95% of the maximum gradient strength in a linear ramp with 32 steps. For each DOSY experiment, the duration of the magnetic field pulse gradients (δ) and the diffusion times (Δ) were optimized to obtain, where possible, 95% signal attenuation for the slowest diffusion species at the last step experiment. For ^1H diffusion experiments, δ values were in the 1.6–6 ms range (for BF_4-samples) and in the 2–6 ms range (for TFSI-samples), while Δ values were 0.6–0.8 s long (for both BF_4- and TFSI-samples). For ^{19}F diffusion experiments, δ values were in the 2.4–6 ms range (for BF_4-samples) and in the 3–6 ms range (for TFSI-samples), while Δ values were 0.6–0.8 s long (for both BF_4- and TFSI-samples). The baselines of all arrayed spectra were corrected prior to processing the data. Data were processed using an exponential filter in F_2 dimension (LB = 0.5 Hz) and integrals were

used in calculating relaxation times. The determination of self-diffusion coefficients used the Bruker T_1/T_2 module of TopSpin for each peak. The precision of the measured diffusion coefficient is estimated to be within 5%.

On equimolar mixtures (samples BF_4-5:5 and TFSI-5:5), 2D NMR rotating frame nuclear Overhauser enhancement (ROESY) and heteronuclear Overhauser effect (HOESY) experiments were recorded at 305 K.

The ^{1}H-^{1}H ROESY experiments were performed by using the phase-sensitive off-resonance 2D ROESY pulse sequence (troesyph in the Bruker library) that minimizes the frequency offset effects. Spectra were recorded using 8 transients over 8192 (t_2) x 1024 (t_1) complex data points. For both samples, 32 dummy scans and a mixing time of 150 ms under the spin lock conditions were used. The relaxation delay was set to 7.4 s for BF_4-5:5 and 5 s for TFSI-5:5. The ROESY data sets were processed by applying a sine squared window function in both dimensions (SSB = 2) prior to the Fourier transform.

The ^{1}H-^{19}F HOESY experiments were acquired using the phase sensitive echo-antiecho pulse sequence (hoesyetgp in the Bruker library). Spectra were recorded using 4 transients over 1024 (t_2) x 128 (t_1) complex data points. For both samples, 32 dummy scans and a 8 s-long relaxation delay were used. For each sample, spectra were acquired at three mixing times (20, 50 and 100 ms). The HOESY data sets were processed by applying a sine squared window function in both dimensions (SSB = 2) and zero-filling to 2048 (t_2) x 256 (t_1) prior to the Fourier transform.

Results and Discussion

Among all IL families, the most widely investigated, for both academic and application goals, have been those based on non-symmetrically substituted *N*,*N'*-dialkylimidazolium cations,

mainly 1-alkyl-3-methylimidazolium-based ILs.[39] $[BF_4]^-$ is one of the most popular anions. In the series of 1-alkyl-3-methylimidazolium tetrafluoroborate salts, $[C_n mim][BF_4]$, those with short alkyl chain lengths (n = 2–10) are liquids at room temperature, whereas the longer chain salts (n = 12–18) are low melting solids with an extensive thermotropic mesophase range.[40] The sample BF_4-10:0 displayed indeed a liquid crystalline phase at temperature below 320 K. None of the BF_4-mixtures showed mesophase transition in the temperature range used in this work. It is worthwhile to note that we also prepared a mixture with a large excess of $[C_{12}mim][BF_4]$, having a molar ratio $[C_{12}mim]^+$:$[C_2mim]^+$ equal to 9.8:0.2, to explore the effect of $[C_2mim]^+$-doping on the liquid crystalline phase. Also in such sample, no stable thermotropic mesophase has been detected. Besides tetrafluoroborate, the anion bis(trifluoromethanesulfonyl)amide $[TFSI]^-$ is largely used, since it forms liquid salts of low viscosity with high thermal and electrochemical stability.[39] In the series of 1-alkyl-3-methylimidazolium bis(trifluoromethylsulfonyl)imide salts, $[C_n mim][TFSI]$, no liquid crystalline phase has been detected.

To get a perspective on the structure and dynamics in the selected mixtures, multiple NMR experiments were performed on samples of Table 1. NMR parameters are clearly affected by the macroscopic properties of the samples, viscosity being probably the most important one. The change in viscosity in $[C_{12}mim][C_2mim][TFSI]$ mixtures and $[C_6mim][C_2mim][BF_4]$ mixtures have been measured.[11,12,24] A discussion on the deviation from ideality of the mixtures is out of the scope of the work, but for the interested reader data from the literature and corresponding analysis in terms of mixing laws are reported in the SI. What is important for the present study is that, in all reported cases, the viscosity decreases with the increase of the molar fraction of the cation having the short alkyl chain (*i.e.* going from pure $[C_{12}mim][TFSI]$ to pure $[C_2mim][TFSI]$ or similarly from pure $[C_6mim][BF_4]$ to pure $[C_2mim][BF_4]$). Even if, to the best of our

knowledge, experimental data on $[C_{12}mim][C_2mim][BF_4]$ mixtures are not available, it is reasonable to assume that also in such system the viscosity will decrease with increasing molar fraction of $[C_2mim]^+$. On the other hand, the macroscopic change in viscosity has been observed qualitatively during sample preparation and is also reflected in terms of linewidth in NMR spectra.

NMR Dynamics

NMR relaxation and self-diffusion studies provide information on the dynamics of ILs and IL mixtures. NMR self-diffusion studies offer molecular level information on the translational motion, whereas the rotational information at the atomic level can be obtained from NMR relaxation studies.[36,37]

Relaxation times T_1 and T_2 and self-diffusion coefficients were measured for both the cation and the anion, using ^1H and ^{19}F NMR, respectively. Note that for the ionic liquid crystal $[C_{12}mim][BF_4]$ the proton relaxation times and diffusion coefficients could be measured only in the isotropic range (325 K and 320 K), while the fluorine values were obtained in the whole compositional range.

In the ^1H spectra of the mixtures (Figs. 2 and S2) most peaks overlap and hence the corresponding relaxation times and diffusion coefficients are an average over the two cation species. The peaks at the lowest field corresponding to the H_2 and $H_{2'}$ protons and the peaks corresponding to H_7 and $H_{17'}$ protons of the terminal methyl groups of the cations (see Fig 1 for atom numbering) are relatively isolated and will be used in the following as representative peaks for each cation, $[C_2mim]^+$ or $[C_{12}mim]^+$, in the mixture

In the ^{19}F spectra a single signal is observed for all the equivalent fluorine atoms in the anions. Note however that the fluorine signal of $[BF_4]^-$ shows two resonances due to the $^{10}B/^{11}B$ isotope effect.

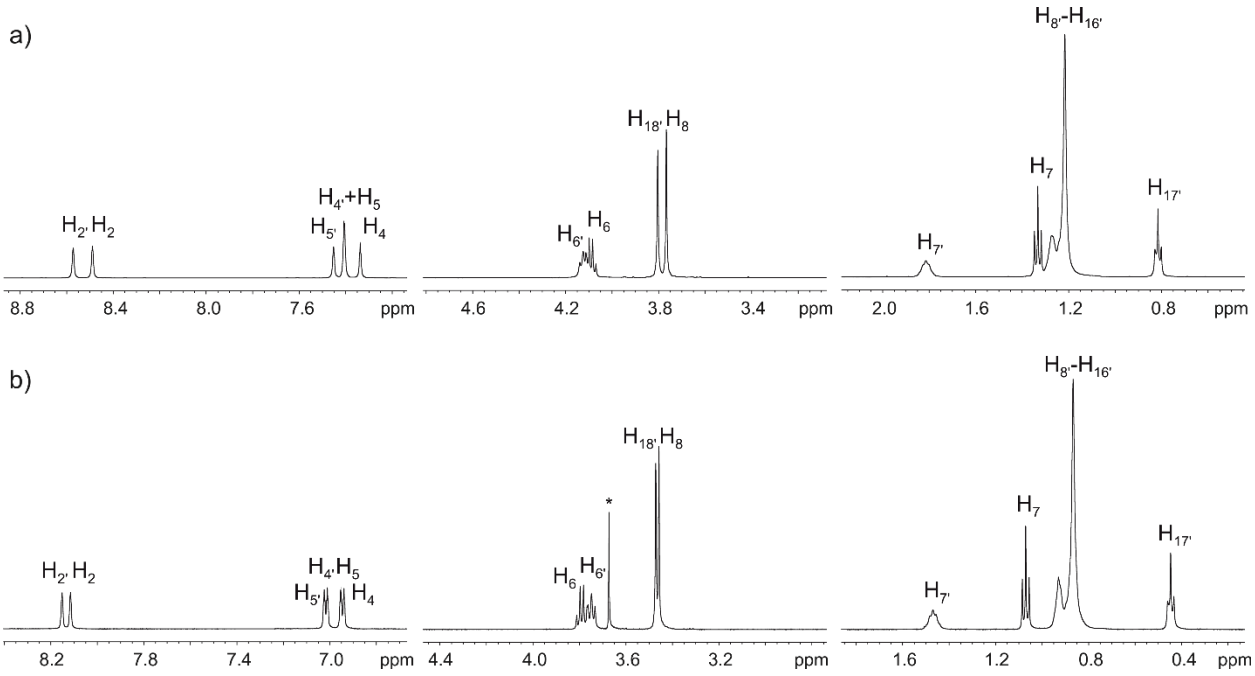

Figure 2. 1D ^1H NMR spectra at 325 K of (a) BF_4-5:5 and (b) TFSI-5:5 (the peak labelled with an asterisk corresponds to an impurity in the capillary).

Rotational dynamics

The spin–lattice (longitudinal, T_1) and spin–spin (transverse, T_2) relaxation times of nuclear spins are sensitive to both intra- and intermolecular relaxation mechanisms and can be used to probe the rotational dynamics of the system. Several NMR active nuclei such as ^1H, ^{13}C, ^{19}F, ^{31}P, ^{14}N, ^{35}Cl, ^2H, ^7Li have been used to characterize pure ILs as well as their mixtures with water and lithium salts.[41–54]

The temperature dependences of ^1H and ^{19}F T_1 and T_2 have been measured in the range 300 – 325 K. In all cases, both T_1 and T_2 increase with the temperature and no T_1 minimum was found

in the considered temperature range. The T_1 and T_2 relaxation times measured for the isolated H_2 and $H_{2'}$ protons of the cations and for the fluorine of the anions in all samples are reported for all temperatures in Tables S1-S3 and Figs. S3-S4 of SI. As an example, Fig. 3 shows the comparison between the T_1 and T_2 values found at 325 K in all samples as a function of the molar ratio of the two components. In all cases, T_1 and T_2 values increase with the increase of the molar fraction of $[C_2mim]^+$, which can be related to the decrease in viscosity of the sample. Within each series (with $[BF_4]^-$ or $[TFSI]^-$ as the anion) the T_1 and T_2 values of proton H_2 of $[C_2mim]^+$ are bigger than those of proton $H_{2'}$ of $[C_{12}mim]^+$. This is due to the size of the cations, with the smaller one ($[C_2mim]^+$) showing a faster rotational motion than the bigger one ($[C_{12}mim]^+$). Comparing the two series, T_1 and T_2 values of the H_2 and $H_{2'}$ protons of both cations are bigger when $[TFSI]^-$ is present as the counterion. To a first approximation, this can be related to the nature of the anion, as $[TFSI]^-$ is well-known for its promotion of fluidity,[10] and gives in general less structured materials compared to $[BF_4]^-$.

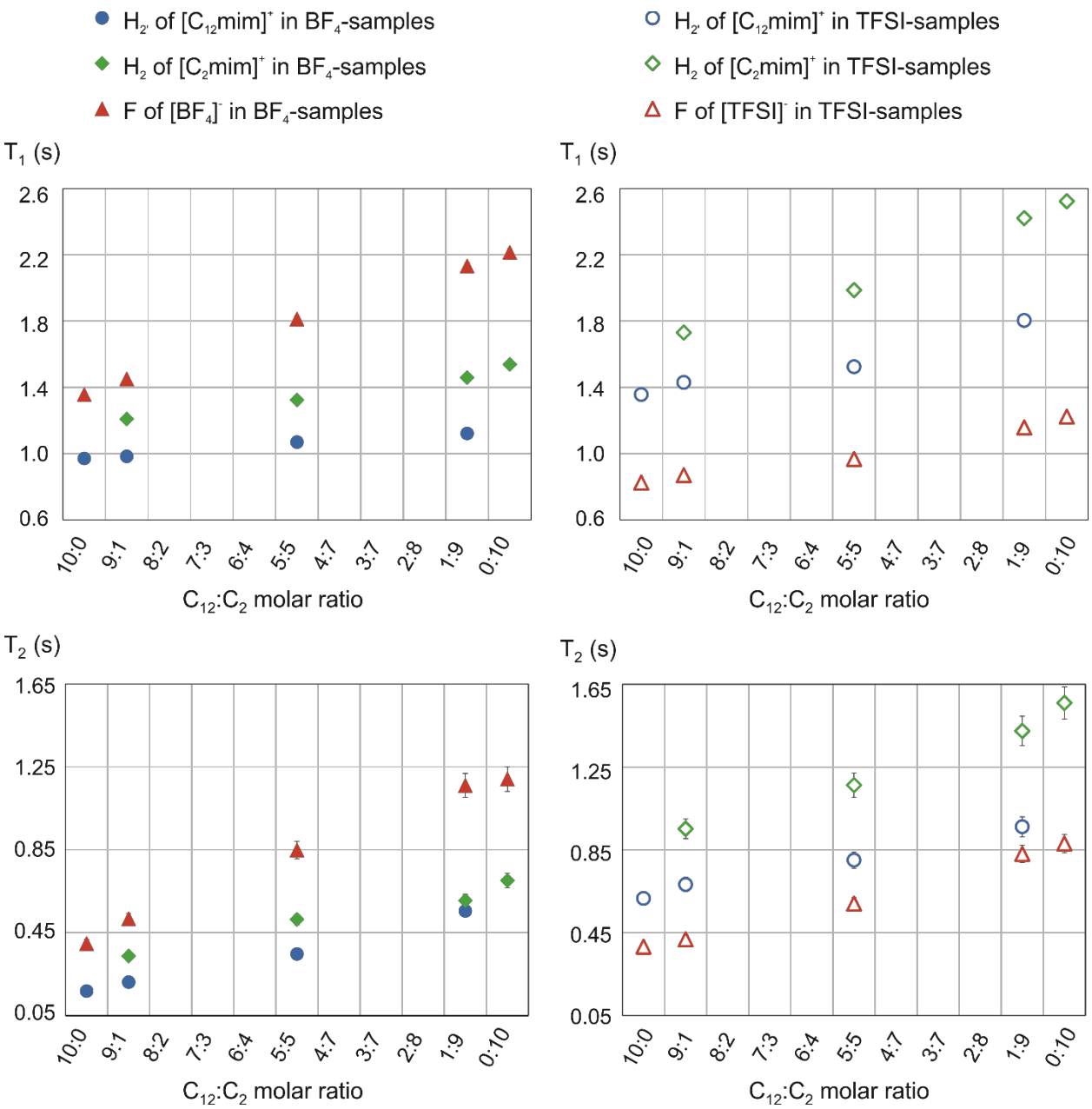

Figure 3. T_1 and T_2 relaxation times measured at 325 K for protons H_2 and $H_{2'}$ of the cations $[C_{12}mim]^+$ and $[C_2mim]^+$ and for fluorine of the anion $[BF_4]^-$ or $[TFSI]^-$ in BF_4-samples (on the left) and TFSI-samples (on the right). T_1 and T_2 are estimated to be accurate within ±1% and ±5%, respectively. When not visible, error bars are within the marker.

A particularly informative parameter is the T_1/T_2 ratio, as it can be used as a very sensitive probe of local order in the system.[55,56] For a common isotropic mixture, T_1/T_2 ratio is equal to 1. Intermediate values close to one are typical of viscous liquids, and higher values indicate the presence of local structures in the system.[55,56] T_1/T_2 ratios calculated for the selected H_2 protons of the cations and for the fluorine of the anions in all samples are reported for all temperatures in Tables S1-S3 and Fig. S5 of SI.

Fig. 4 reports the T_1/T_2 ratios calculated for the fluorine of the anions in all samples at all experimental temperatures. It can be observed that in both cases the T_1/T_2 ratio progressively decreases with increasing temperature and increasing molar fraction of the smaller cation ($[C_2mim]^+$). The maximum T_1/T_2 value found when $[TFSI]^-$ is the counterion (at 300 K and for a C_{12}:C_2 molar ratio of 10:0) is 4.1, whereas it is of 11.1 for $[BF_4]^-$. This is a confirmation of the significantly more ordered nanostructure formed with tetrafluoroborate. It has been reported for different ILs that T_1/T_2 ratios between 1.0 and 2.6 are not sufficiently high to confirm the presence of sustained local order on a time scale of the inverse Larmor frequency of the nucleus under study.[56,57] In the samples studied in this work, we can observe that the TFSI-mixtures behave overall as an isotropic medium in the whole compositional range on the timescale of $\sim 1/\omega$, with T_1/T_2 ratios between 1.4 to 4.4. On the contrary, T_1/T_2 ratios found for BF_4-mixtures point toward the existence of local structures formed on the timescale of $\sim 1/\omega$ in the samples with a significant amount of $[C_{12}mim]^+$ (BF_4-10:0, BF_4-1:9, BF_4-5:5) and at the lowest temperatures.

For comparison, the T_1/T_2 ratios calculated for the H_2 and $H_{2'}$ protons of the cations in all samples at all experimental temperatures are reported in Fig. S6.

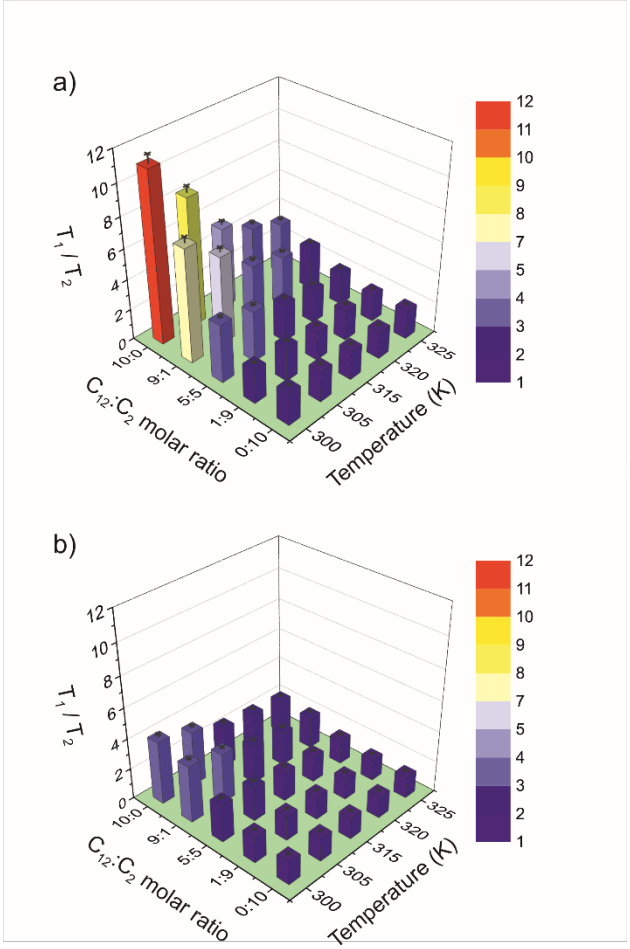

Figure 4. T_1/T_2 ratios calculated for the fluorine of the anions (a) $[BF_4]^-$ and (b) $[TFSI]^-$ in all samples. T_1/T_2 are estimated to be accurate within ±5%.

From temperature-dependent T_1 data it is possible in principle to calculate the activation energy of the rotational motion at a given site when $\omega_0\tau_C \ll 1$ (see SI for the theoretical background).[48] It should be noted that ionic liquids may show strong deviations from Arrhenius behaviour when relaxation measurements over wide temperature ranges are performed.(Becher and Vogel 2019). However, in the present work a quite narrow temperature range has been considered and to a first approximation the temperature-dependent correlation time τ_C obeys the Arrhenius equation (Figs. S7-S8). It is thus possible to estimate the activation energy of

reorientational motion in the studied temperature interval.(Shimizu 2016) An additional noteworthy point here is that structurally different protons may exhibit different T_1 values, as the result of characteristic intramolecular dynamics of the given segment, which contribute to the relaxation, in addition to the overall reorientation of the cation. (Becher and Vogel, JCP 151, 194503 (2019)). It follows that one can calculate an "apparent" activation energy averaged over several types of movements.(Bystrov 2019). The apparent activation energy of the rotational motion, E_a^{rot}, estimated from the linear dependence of T_1 relaxation times in the range 300-325 K for protons H_2 and H_7 of $[C_2mim]^+$, protons $H_{2'}$ and $H_{17'}$ of $[C_{12}mim]^+$, and ^{19}F of $[BF_4]^-$ and $[TFSI]^-$ are given in Table 2 and Figure S9. Note that in the BF_4-mixtures the signal corresponding to proton H_7 is close to the intense signal from the methylene protons of the long alkyl chain of $[C_{12}mim]^+$, so that the integration of the isolated peak was not possible for BF_4-9:1.

Table 2. Apparent activation energies E_a^{rot} (kJmol^{-1}) obtained from temperature-dependent T_1 relaxation times in the range 300-325 K at given proton and fluorine sites for the pure ILs and their mixtures. Values are estimated to be accurate within ±5%.

	BF_4-mixtures				
C_{12}:C_2 molar ratio	$H_{2'}$ of $[C_{12}mim]^+$	H_2 of $[C_2mim]^+$	$H_{17'}$ of $[C_{12}mim]^+$	H_7 of $[C_2mim]^+$	$[BF_4]^-$
10:1					[a]
9:1	6.9	7.1	16.3	[a]	8.8
5:5	6.2	5.5	13.7	11.5	9.2
1:9	5.3	8.1	13.6	13.6	8.2
0:10		9.3		14.1	7.9

	TFSI-mixtures				
C_{12}:C_2 molar ratio	H_2, of $[C_{12}mim]^+$	H_2 of $[C_2mim]^+$	H_{17}, of $[C_{12}mim]^+$	H_7 of $[C_2mim]^+$	$[TFSI]^-$
10:1	11.7		13.9		9.1
9:1	8.8	9.6	13.6	11.3	11.6
5:5	7.7	9.4	13.0	13.8	12.7
1:9	8.5	10.4	13.3	14.2	13.9
0:10		11.9		23.8	14.5

[a] Values not available

Note that local reorientation processes affect to some extent the relaxation data of the selected protons, (Bystrov 2019, Becher and Vogel 2019) and the same holds also for ^{19}F relaxation data, largely governed by CF_3 and BF_4 reorientations. Therefore, the results should be interpreted bearing in mind that structural relaxation and intramolecular motion overlaps, but can anyway give some insights into segmental reorientation. Moreover, from the T_1/T_2 ratio we can assume that in the TFSI-mixtures the extreme narrowing approximation can be applied, but the BF_4-mixtures might locate more in the intermediate region, at least for some compositional ranges, than the E_a^{rot} may be biased.[50] However, the order of magnitude found here for the activation energies are in line with data from the literature. For instance, for [C_1mim][TFSI] the E_a^{rot} estimated from the linear part of the proton T_1 curve (from 233 to 293 K) at low field in the crystalline state was of approximately 8.7 kJ mol^{-1}, and was associated with the rotational motion of methyl group.[47] An E_a^{rot} of 12.5−15.1 kJ mol^{-1} was also found for the crystalline states of [C_4mim][PF_6] and assigned to the δ-CH_3 rotation.[58] In ILs composed of N-methyl-N-propyl-pyrrolidinium (P_{13}) with two anions, TFSI and FSI, the three-type protons have similar activation energies (ca. 15 kJ/mol-1 for FSI-systems and 17 kJ/mol^{-1} for TFSI systems).[59] E_a^{rot} for alkyl

protons of $[C_4mim][BF_4]$ calculated from temperature-dependent spin-lattice relaxation rate at the different sites were in the range 15-19 kJ/mol,[51,60] and E_a for H_7 of $[C_2mim][BF_4]$ was 16.1 kJ/mol.[60] As for the fluorine, the activation energy calculated from ^{19}F T_1 values was ca. 14 $kJmol^{-1}$ (above 303K) in $[P_{13}][TFSI]$, 14.1 $kJmol^{-1}$ (above 283K) in $[C_2mim][TFSI]$, 11.5 $kJmol^{-1}$ (above 288 K) in $[C_4mim][BF_4]$, and 10.8 $kJmol^{-1}$ (above 303 K) in $[C_2mim][BF_4]$.[46,59,60]

Therefore, while bearing in mind the restriction of the obtained apparent activation energies in the considered temperature range, a number of considerations can be drawn from Table 2, :

- E_a^{rot} for $[BF_4]^-$ (7.9-9.2 $kJmol^{-1}$) are smaller than E_a^{rot} for $[TFSI]^-$ (9.1-14.5 $kJmol^{-1}$). This suggests that the rotational motion can be activated more easily for $[BF_4]^-$ than $[TFSI]^-$, due to the smaller ion size and the tetrahedral symmetrical structure.[60]
- E_a^{rot} for $H_{17'}$ in both BF_4- and TFSI-mixtures slightly decreases with increasing $[C_2mim]^+$ molar fraction, and in TFSI-mixtures it is almost independent on the composition of the mixture (13.9-13.0 $kJmol^{-1}$). This can be explained considering that the terminal methyl group of the long chains feels always a very similar environment, that is the apolar chains of the neighbouring cations. In other words, even if the progressive increase of the smaller cation affects the whole nanostructure of the system, the inner core of the polar domains does not change dramatically. On the contrary, E_a^{rot} for H_7 increases, more markedly in TFSI-mixtures (11.3-23.8 $kJmol^{-1}$). This is because the small cations are located mostly in the polar domain, which suffers more significantly from the change in the molar ratio between the smaller and the bigger cation.
- Similar considerations on the local environment are difficult to be drawn from the apparent activation energies of protons H_2 and $H_{2'}$, whose trends are not clear.[non saprei come

decifrare questi andamenti, e non so se ha senso scrivere qualcosa del genere o semplicemente glissare]

- A clear increase in E_a^{rot} is also seen for ^{19}F in TFSI mixtures (9.1-14.5 kJmol^{-1}), in line with the trend for H_7. Contrarily, E_a^{rot} for ^{19}F in BF_4 mixtures is almost constant.

The latter point is likely the most striking finding. If interpreted together with results for the two cations, the different behaviour displayed by the two anions would indicate that $[BF_4]^-$ is located steadily in the polar domain, whose inner composition and arrangement do not change significantly with the change in the molar ratio of the two components. This would explain why the activation energy required for a substantially local motion does not vary and confirms the role of $[BF_4]^-$ as a strong counterion. The scenario is different for the more conformationally flexible anion with extensive charge delocalization, $[TFSI]^-$, which probe both polar and apolar domains and is then sensitive to the nanostructural modifications that occur upon dilution of $[C_{12}mim][TFSI]$ with $[C_2mim][TFSI]$. The effect of "encroachment" has been already observed for anions such as $[TFSI]^-$ and related both to the size, which exceeds that of the imidazolium heads, and to the low basicity, which reduces the strength of the polar interactions.[31] Overall, this translates into a weakly interacting nature of the anion that easily oversteps the bounds of the polar domains toward the apolar chains. Even considering that the proposed T_1 analysis produce apparent E_a^{rot} values in a narrow temperature range, the results for the two series reveal a substantially different behaviour of the two anions and could be read as a dynamic fingerprint of the short-range mobility in IL mixtures.

Translational dynamics

Pulsed Field Gradient (PFG) NMR has been largely used to measure diffusion in several ILs and IL mixtures.[9,10,29,38,43,55,59,61–70] The self-diffusion coefficients D of the anions and cations in all the samples were measured independently by PFG experiments in the ^{19}F and ^{1}H frequency domains, respectively. The resulting self-diffusion coefficients are reported for all temperatures in Tables S5-S7 and Fig. S10 of SI.

Fig. 5 shows as an example the comparison between the diffusion coefficients found at 325 K for the cations $[C_{12}mim]^+$ and $[C_2mim]^+$ and the anions $[BF_4]^-$ and $[TFSI]^-$ in all samples as a function of the molar ratio of the two components of the mixtures. In all cases, the mobility increases with the increase of the molar fraction of the cation with the shorter chain ($[C_2mim]^+$) in the mixture. Again, this observation can be explained by the decrease in the viscosity of the mixture, as also observed in other IL mixtures.[32]

As previously found,[62] in neat ILs the self-diffusion coefficients of cations are faster than those of the anion in the $[C_2mim]^+$-samples and slower in the $[C_{12}mim]^+$-samples. For the series of $[C_nmim][TFSI]$ ILs, it has been reported that the self-diffusion coefficients of cations are faster as compared to the anion in shorter alkyl group substitution ILs and slightly slower in longer alkyl group substitution ILs, with a crossover in hexyl or octyl (n = 6-8) group substitution.[62] (Becher and Vogel 2019) Here the system is complicated by the simultaneous presence of two cations, one with a short ethyl chain, and the other with a long dodecyl chain. In all mixtures, the self-diffusion coefficients of the anion turned out to be an intermediate value between those of the two cations.

Comparing the two series, in the neat ILs with the longer chain ($[C_{12}mim][BF_4]$ and $[C_{12}mim][TFSI]$) and in all mixtures (9:1, 5:5 and 1:9), both cations diffuse faster when $[TFSI]^-$ is present as the counterion with respect to $[BF_4]^-$. To a first approximation, this can be related to

the nature of the anion, as $[TFSI]^-$ gives in general more fluid and less structured materials compared to $[BF_4]^-$. As for the anions, it can been observed that $[TFSI]^-$ diffuses faster than $[BF_4]^-$ in the neat ILs with the longer chain ($[C_{12}mim][BF_4]$ and $[C_{12}mim][TFSI]$) and in the mixtures with C_{12}:C_2 molar ratios equal to 9:1 and 5:5. Both anions have similar diffusion coefficients in the neat ILs with the shorter chain ($[C_2mim][BF_4]$ and $[C_2mim][TFSI]$) and in the mixture with C_{12}:C_2 molar ratio equal to 1:9.

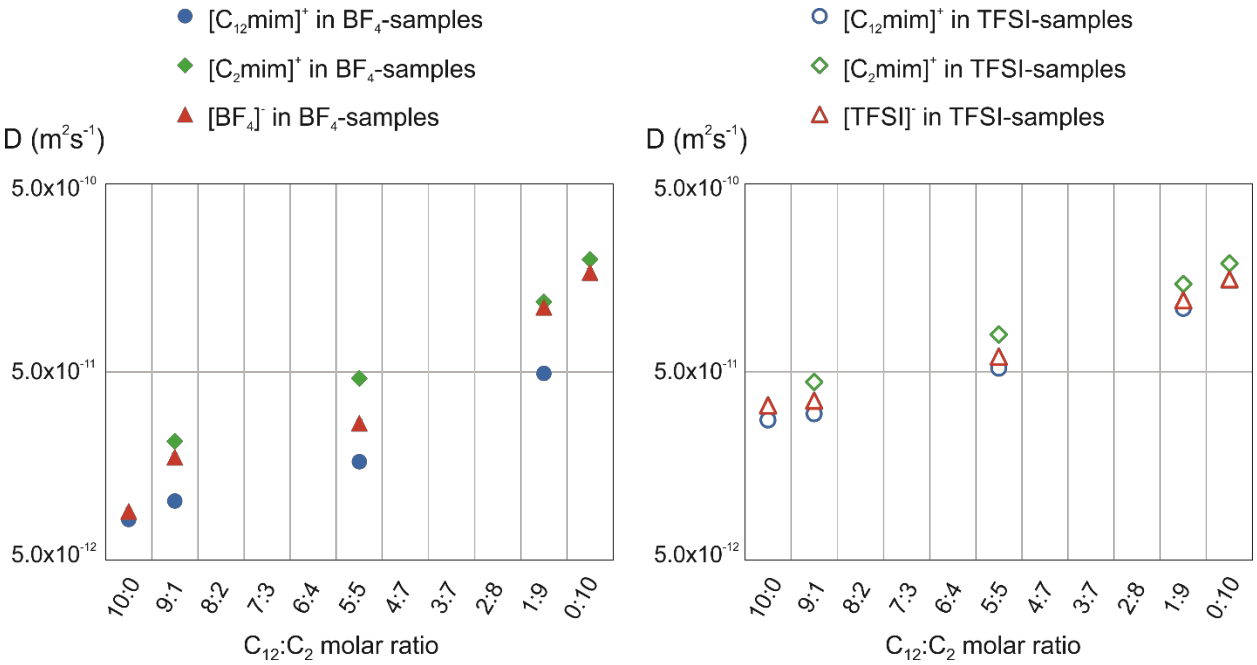

Figure 5. Diffusion coefficients measured at 325 K for the cations $[C_{12}mim]^+$ and $[C_2mim]^+$ and the anion $[BF_4]^-$ or $[TFSI]^-$ in all samples. *D* are estimated to be accurate within ±5%. When not visible, error bars are within the marker.

The dependence of the transport properties of the mixtures against temperature was also investigated. A linear Arrhenius temperature behaviour has been observed for the diffusion coefficients of all samples over the 300–325 K temperature range (Figs. S11). Note again that the Arrhenius behaviour depends strongly on the location of the considered temperature interval with

respect to the transition temperatures of the material, and strong deviations from the Arrhenius law have been described for neat [$C_n$mim][TFSI] ILs.over wide temperature ranges (Becher and Vogel 2019). As expected, the diffusion coefficient for the anion in the neat ionic liquid crystal [C_{12}mim][BF_4] does not change linearly with the temperature over the 300-325 K range, but a somehow linear trend can be observed in the anisotropic range 315-300 K. The apparent activation energies calculated from ion diffusion measurements are listed in Table 3 and displayed in Fig S12 as a function of the molar ratio of the two component of the mixtures (see SI for theoretical background).

Table 3. Apparent activation energies E_a^{transl} (kJmol^{-1}) obtained from temperature-dependent diffusion data for the pure ILs and their mixtures. Values are estimated to be accurate within ±5%.

	BF_4-mixtures			TFSI-mixtures		
C_{12}:C_2 molar ratio	$[C_{12}mim]^+$	$[C_2mim]^+$	$[BF_4]^-$	$[C_{12}mim]^+$	$[C_2mim]^+$	$[TFSI]^-$
10:1			49.3[a]	43.5		44.1
9:1	51.7	55.4	51.7	41.9	40.5	41.3
5:5	42.1	38.2	39.0	41.5	37.0	40.7
1:9	44.0	32.3	35.8	44.3	34.8	44.7
0:10		40.6	42.3		37.3	46.6

[a] Calculated only in the anisotropic range.

In all cases, the activation energy is not linear but shows a minimum value at a given composition. The change of the activation energy in the studied compositional range is greater for BF_4-mixtures than for TFSI-mixtures. However, the trends found for the two cations are quite

similar in the two series. The smaller cation $[C_2mim]^+$ shows the lowest E_a^{transl} for the samples BF_4-1:9 and TFSI-1:9, while the minimum is observed for the equimolar mixtures (BF_4-5:5 and TFSI-5:5) in the case of the bigger cation $[C_{12}mim]^+$. Next to the viscosity effect, which decreases going from pure $[C_{12}mim][X]$ to pure $[C_2mim][X]$, to rationalise these trends one could consider also the "disturbing effect" exerted by the addition of a cation with different size to a pure IL. This means that when a 10 mole percent of $[C_{12}mim][X]$ is added to pure $[C_2mim][X]$, the structure of the IL is disturbed so that the small cation moves slightly more easily in the 1:9 mixture. Viceversa if one considers the addition of a small cation to pure $[C_{12}mim][X]$, the effect is not that strong until the molar fraction of $[C_2mim]^+$ gets significant.

Comparing the E_a^{transl} of the two anions in the two series, a markedly different behaviour emerges again. In BF_4-mixtures, the diffusive motion of the anion appears to be strongly correlated with that of the smaller cation in all mixtures but the sample with a higher molar ratio of $[C_{12}mim]^+$ (BF_4-9:1), where $[BF_4]^-$ and $[C_{12}mim]^+$ have the same activation energy. In TFSI-mixtures, the anion $[TFSI]^-$ and the cation with the longer chain ($[C_{12}mim]^+$) have very similar activation energies in the whole compositional range, with slight changes and a minimum value for the sample TFSI-5:5. The diffusive motion of the smaller cation $[C_2mim]^+$ appear to be less correlated and its activation energy is always smaller. The E_a^{transl} of the anion can be seen then as an important dynamic probe in IL mixtures: the larger and more diffuse $[TFSI]^-$ explores both polar and apolar domains and its diffusive motion follows more tightly that of the amphiphilic cation, while the smaller and charge localized $[BF_4]^-$ moves rather within the polar regions so that its diffusive motion is closer to that of $[C_2mim]^+$.

Finally, it should be noted that in the considered temperature interval the apparent activation energies associated to relaxation data are of 5–24 kJ/mol (see Table 2) and the apparent

activation energies associated to diffusion data are larger (32-52 kJ/mol) (see Table 3). Such difference is not surprising if one considers the molecular motion that affect these apparent activation energies, rotational vs translational, and is in agreement with values found for other ILs. For instance in P_{13}-FSI e P_{13}-TFSI the activation energies were 15–18 kJ/mol for the rotational motion and much larger for translational diffusion (25 kJ/mol for P_{13}-FSA and 30 kJ/mol P_{13}-TFSA).[59] Indeed, it should be remembered again that what dominates the observed T_1 data is not the correlation time of the reorientation of the ion as a whole, but the characteristic time for the rotation of a segment. In this sense, the T_1 and D analysis can be seen as complementary tools to probe the dynamics of the system at different scales.

NMR structure

Valuable information for the assessment of the local structure of ionic liquids, including ion-ion interactions, can be obtained from the intermolecular Nuclear Overhauser Enhancement (NOE).[71] The NOE originates from dipolar cross-relaxation between nuclear pairs and thus gives information on the proximity between the molecular sites involved in the interactions. In the investigated mixtures, relative proximities for cation-cation and cation–anion interactions were studied separately by means of two 2D experiments: {^{1}H-^{1}H} rotating frame NOE correlation (ROESY) and {^{1}H-^{19}F} heteronuclear NOE correlation (HOESY) experiments, as they contain different nuclides with I = 1/2.

The interpretation of the NOE data for ILs showed a rapid evolution from the atom-pairs interpretation based on short-distance interactions,[71–75] to a generalized model including also long range effects, first introduced by Weingärtner in 2013.[76] The authors demonstrated that intermolecular NOEs were influenced by the Larmor frequency of the interacting nuclei, with the

important fall-out that the intermolecular NOEs of nuclei with similar Larmor frequency – such as in {^{1}H-^{1}H} or {^{1}H-^{19}F} NOE experiments – explore not only the first neighbour contacts but also long-range interactions. Additionally, different HOESY experiments are expected to provide different type of distance-dependent information on the interacting atoms as a function of their relative Larmor frequencies. For example, in Li^{+} doped ILs with fluorine containing anions, typically employed for electrochemical applications, {^{1}H-^{1}H} and {^{1}H-^{19}F} contain information interaction distances beyond the conventional threshold of 4 Å for vanishing NOE, while {^{1}H-^{7}Li} NOEs are largely dominated by short-range interactions.[77,78]

^{1}H-^{1}H proximity: homonuclear experiments (ROESY)

^{1}H-^{1}H ROESY is one of the 2D NMR methods for correlating signals arising from protons close in space.[79] The ROESY correlation peaks are the result of cross-relaxation between neighbouring protons, the main mechanism being the through-space dipole–dipole interaction. The cross-peak intensity reflects the extent of magnetization transfer between interacting nuclei and, in the case of intramolecular NOE, *i.e.* in the case of fixed internuclear distances, it is inversely proportional to the sixth power of their internuclear distance. According to the Weingärtner model, the intermolecular NOE are frequency dependent and also affected by time-dependent internuclear distances. In other words, the internuclear distances are modulated by the rotational and translational dynamic properties of the ions, leading to a distance dependence of NOE no longer scaling as r^{-6}, but rather as r^{-n} with typically $1 < n < 6$. The quantitative extraction of intermolecular distances *via* intermolecular NOEs is not the focus of this work and it is thoroughly described by Martin *et al.*.[80] As a consequence of the r^{-n} distance scaling of the intermolecular NOEs, their intensity spots on spins far beyond the first coordination layer. This

would mean that site-specific NOE measurements reflect the mean orientation of the ions over long distances rather than the local structure of distinct ion aggregates.

In the present work, we used $^{1}H–^{1}H$ NOE data to provide details on the inter-molecular cation–cation organization in the studied mixtures by a qualitative evaluation of the cross-peaks among the different protons of the two components.

Figure S13 shows the ROESY spectrum recorded at 305 K for the sample BF_4-5:5. The pattern is overall similar to that found for neat [$C_n$mim]-based ILs with n = 6, 8 and in general the ROESY cross-peaks evidence an IL molecular organization close to that already proposed for other neat 1-alkyl-3-methylimidazolium salts with aromatic ring associations and possible head-to-tail and tail-to-tail contacts.[72,81]

From the standpoint of the IL mixture, it is interesting to find evidence of intermolecular correlations between the two types of cations. Many proton signals are overlapped in ^{1}H NMR spectra of BF_4- and TFSI-mixtures, making the assignment of many cross-peaks ambiguous. Luckily, in the aromatic part, peaks are not fully overlapping, and cross-peaks in this area can give hints on the nanostructural organization of the mixture. Indeed, the cross-peaks between H_2 of $[C_2mim]^+$ and $H_{5'}$ of $[C_{12}mim]^+$ and between $H_{2'}$ of $[C_{12}mim]^+$ and H_4 of $[C_2mim]^+$ reasonably suggest the presence of intermolecular interactions between the two different cations and thus implies the existence of mixed ring assemblies (see inset in Fig S13). Note that due to the overlap of signals corresponding to H_5 of $[C_2mim]^+$ and $H_{4'}$ of $[C_{12}mim]^+$ we would rather avoid any interpretation of the corresponding cross-peaks. The main conclusion emerging from the observed $^{1}H–^{1}H$ NOEs in the equimolar BF_4-5:5 mixture is that the cations' heads show significant short contacts despite the repulsive coulombic interaction, in line with the existence of polar domains in the mixture.

The ROESY spectrum recorded at 305 K for the sample TFSI-5:5 is somehow different (Figure S14). ROESY cross-peaks are detectable between H_2 and H_4, and H_2 and H_5 of $[C_2mim]^+$, or between $H_{2'}$ and $H_{5'}$ of $[C_{12}mim]^+$ (see inset in Fig S14). Such ring intermolecular interactions between the same cations are compatible with the formation of polar domains. This observation is substantiated by the presence of cross-peaks between H_2 and H_6, H_2 and H_8, H_4 and H_8, and H_5 and H_6 of $[C_2mim]^+$, or similarly between $H_{2'}$ and $H_{18'}$, $H_{2'}$ and $H_{6'}$, $H_{4'}$ and $H_{18'}$, and $H_{5'}$ and $H_{6'}$ of $[C_{12}mim]^+$ (see inset in Fig S14). No clear ROESY peaks between signals of the two different cations are observed here.

The overall picture seems to indicate a quite different situation in the two equimolar mixtures, with the BF_4-sample showing clean ROESY peaks between the ring's protons of both the same and different cation species, and the TFSI-mixture providing evidence of some interactions between the same cation species but no clear intermolecular contacts between $[C_2mim]^+$ and $[C_{12}mim]^+$.

In summary, the presence or absence of intermolecular NOE interactions between the two types of cations in BF_4- or TFSI-mixture, respectively, might point toward a different nanostructure in the two sample. In the BF_4-mixture the small $[C_2mim]^+$ cation would be well intercalated between the $[C_{12}mim]^+$ heads, resulting in an intimate and "well-mixed" ring assemblies. In the TFSI-mixture, interactions are in general looser because of the anion's nature, and pretty ordered $[C_{12}mim]^+$-$[C_{12}mim]^+$ assemblies are formed, while the small cation $[C_2mim]^+$ would be probably too mobile to give detectable interactions with the $[C_{12}mim]^+$.

^{1}H-^{19}F proximity: heteronuclear experiments (HOESY)

This section reports on heteronuclear {^{1}H-^{19}F} 2D NOE spectroscopy (HOESY) to investigate anion-cation interactions by exploiting the fact that cations contain ^{1}H but not ^{19}F nuclei and viceversa for the anions.

Figure 6 shows the HOESY spectra of the two equimolar mixtures BF_4-5:5 and TFSI-5:5 acquired at three different mixing times. The cross signals between the protons of the cations and the fluorine nuclei of the anions are recognisable. All cation peaks of IL are interacting with the anion. The individual signal intensities give an idea of the order of magnitude of the particular cross relaxation and thus of the intensity of interaction. Even if a quantitative analysis of HOESY cross-peaks is out of the scope of the present work, to qualitatively interpret the HOESY spectra, the cross-peak were integrated and the integrated HOESY intensities corrected by a factor $n_H n_F/(n_H + n_F)$, with n_H and n_F the number of ^{1}H and ^{19}F nuclei contributing to the observed NOE signal.[69,82,83] Original and corrected cross-peak volumes are reported in Tables S8-S9 and Figure 7. In particular, the histograms of Fig. 7 are the result of the grouping of NOE contribution from different molecular sites. The histogram bars labelled as H_2, $H_{2'}$, H_4, $H_{4'}$, H_5, $H_{5'}$, H_6, $H_{6'}$, H_8 and $H_{18'}$ correspond to the NOE between the fluorine nuclei of the anion and the protons on the polar domain of the ILs. The bar on the right hand corner of the plot is labelled as “apolar” and accounts for the cumulative NOE intensity between the fluorine nuclei of anion and all of the protons belonging to the alkyl chain of the cation and not contributing to the polar domain. In this way the histograms offer a clear picture of the proximity of the anion to both domains of the ILs for both $[BF_4]^-$ and $[TFSI]^-$. As expected, in sample BF_4-5:5 the strongest interaction is with the head group and only weak interactions can be observed with the alkyl chain. The situation is different in TFSI-5:5, where the most significant interactions are observed between the anion and the alkyl chain, similar to what reported for $[C_8mim][TFSI]$.[82]

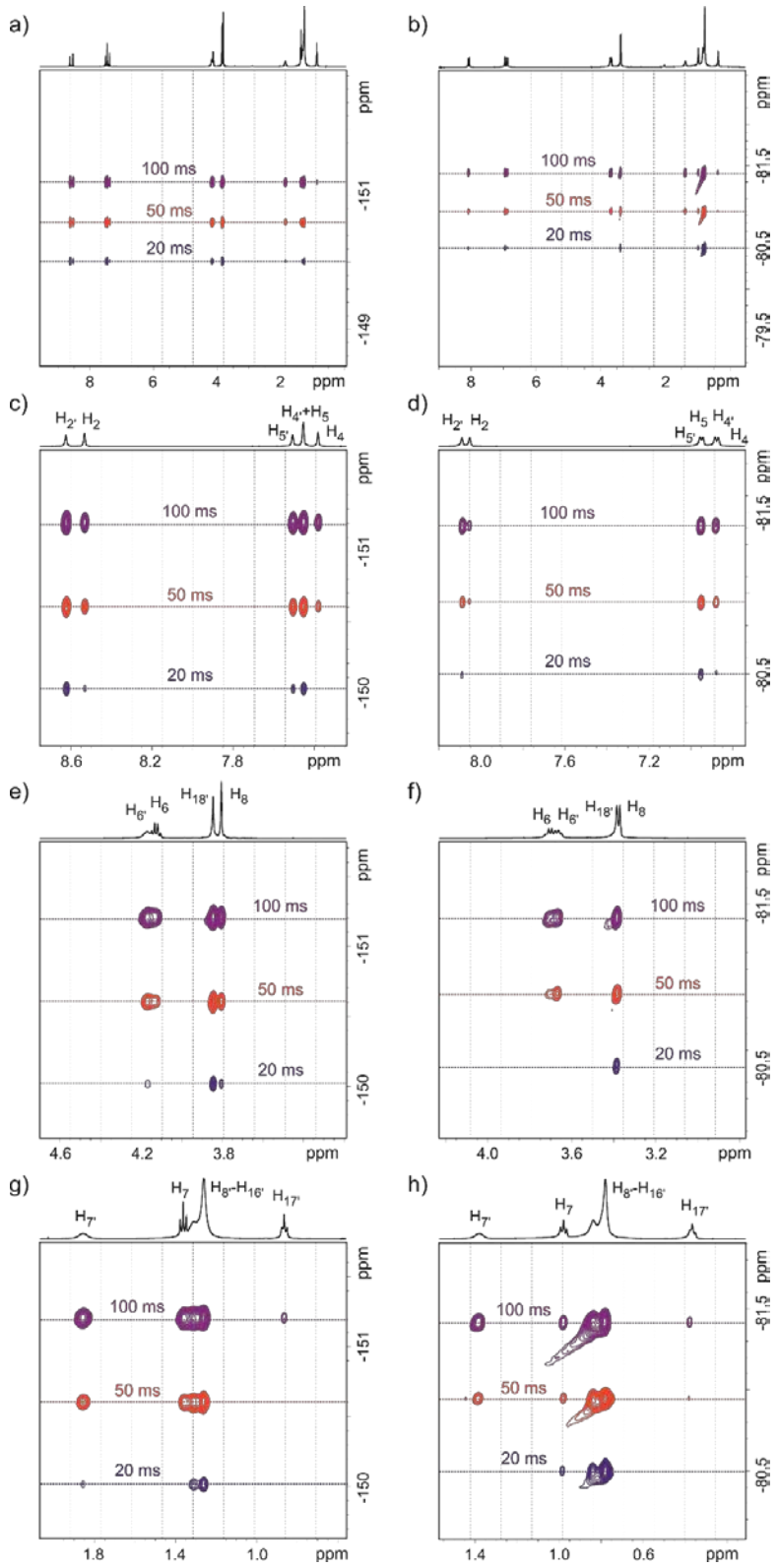
a)
b)
c)
d)
e)
f)
g)
h)
100 ms
50 ms
20 ms
ppm
H2' H2
H4'+H5
H5'
H4
H5 H4'
H6' H6
H18'
H8
H7'
H7
H8'-H16'
H17'

Figure 6. HOESY spectra at different mixing times (20, 50 or 100 ms) recorded at 305 K for (a) BF_4-5:5 and (b) TFSI-5:5, and enlargements of the different spectral regions (c-h).

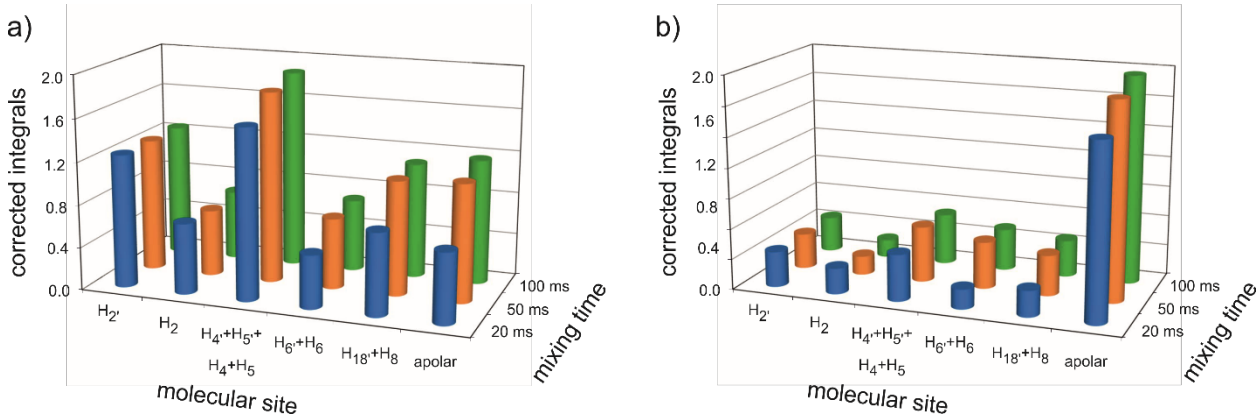

Figure 7. Corrected integrated peak volume of ^{1}H-^{19}F NOE cross peaks at 20, 50 and 100 ms mixing time for (a) sample BF_4-5:5 and (b) sample TFSI-5:5. See text for a description of the labels.

Conclusions

We showed how a joint use of different NMR-derived descriptors – T_1/T_2 ratios, activation energy for T_1 and for diffusion, homo- and heteronuclear intermolecular NOEs – contributes to a description of the polar and apolar domains in representative ILs mixtures, underlining the role of the anion in dictating the dynamic features of the mixtures. The anions used in this study are paradigmatic of opposite classes: small, symmetric, charge localized in one case ($[BF_4]^-$), and large, with conformation degrees of freedom, diffuse and polarizable charge in the other ($[TFSI]^-$). The results above discussed coherently describe two different solvation modes of the anions: $[BF_4]^-$ dominated by coulombic interactions with the polar heads (quite irrespective of the average alkyl chain length in the mixtures), and $[TFSI]^-$ sensitive to a complex balance of coulombic and dispersive interactions that allows extensive interaction with the palisade of the

alkyl chains aggregation typical of the apolar domains. On the other way round, the relaxation and diffusion data can be used to validate the structural interpretation provided by the NOE data without passing through the rigorous but time-consuming protocol of full simulation of the build-up curves leading to the assessment of nuclei-pair distances. This point is quite important in view of a re-thinking of the intermolecular NOE interpretation considering also the long-range effects. Finally, and from a methodological standpoint, the structural features of the anions remarked above, and their response to the NMR descriptors used in this work, indicate that those anions can be exploited as "dynamic probes" for gaining information of the polar and non-polar regions of ionic liquids and their mixtures.

ASSOCIATED CONTENT

Supporting Information.

The following files are available free of charge.

Brief survey of reported viscosity data; ^{1}H and ROESY spectra; tables and plots reporting experimental T_1, T_2, T_1/T_2, and D values; plots of rotational and translational activation energies; tables reporting integrals from HOESY spectra; theoretical background for the calculation of activation energy from relaxation and diffusion data (PDF file)

AUTHOR INFORMATION

Corresponding Author

*E-mail: mariaenrica.dipietro@polimi.it. Phone +39 02 2399 3045 (M.E.D.P.).

*E-mail: andrea.mele@polimi.it. Phone +39 02 2399 3006 (A.M.).

Author Contributions

The manuscript was written through contributions of all authors. All authors have given approval to the final version of the manuscript.

ACKNOWLEDGMENT

MEDP thanks Politecnico di Milano for her postdoctoral fellowship in the framework of the "MSCA EF Master Class 2018" funding programme.

ABBREVIATIONS

BPP-LED, bipolar pulse longitudinal eddy current delay; CPMG, Carr-Purcell Meiboom-Gill; DMSO, dimethyl sulfoxide; DOSY, diffusion ordered spectroscopy; HOESY, heteronuclear Overhauser enhancement spectroscopy; ILs, ionic liquids; IR, inversion recovery; NMR, nuclear magnetic resonance; NOE, nuclear Overhauser enhancement; PFG, pulsed field gradient; PGSE, pulse gradient spin echo; ROESY, rotating frame nuclear Overhauser enhancement.

REFERENCES

1. Niedermeyer H, Hallett JP, Villar-Garcia IJ, Hunt PA, Welton T. Mixtures of ionic liquids. *Chem Soc Rev*. 2012;41(23):7780-7802. doi:10.1039/c2cs35177c

2. Welton T. Ionic liquids: a brief history. *Biophys Rev*. 2018;10(3):691-706. doi:10.1007/s12551-018-0419-2

3. Cabry CP, D'Andrea L, Shimizu K, et al. Exploring the bulk-phase structure of ionic liquid mixtures using small-angle neutron scattering. *Faraday Discuss*. 2018;206:265-289. doi:10.1039/c7fd00167c

4. Hallett JP, Welton T. Room-temperature ionic liquids: Solvents for synthesis and catalysis. 2. *Chem Rev*. 2011;111(5):3508-3576. doi:10.1021/cr1003248

5. Plechkova N V., Seddon KR. Applications of ionic liquids in the chemical industry. *Chem Soc Rev*. 2008;37(1):123-150. doi:10.1039/b006677j

6. Watanabe M, Thomas ML, Zhang S, Ueno K, Yasuda T, Dokko K. Application of ionic liquids to energy storage and conversion materials and devices. *Chem Rev*. 2017;117(10):7190-7239. doi:10.1021/acs.chemrev.6b00504

7. Chatel G, Pereira JFB, Debbeti V, Wang H, Rogers RD. Mixing ionic liquids-"simple mixtures" or “double salts”? *Green Chem*. 2014;16(4):2051-2083. doi:10.1039/c3gc41389f

8. Clough MT, Crick CR, Gräsvik J, et al. A physicochemical investigation of ionic liquid mixtures. *Chem Sci*. 2015;6(2):1101-1114. doi:10.1039/c4sc02931c

9. Miran MS, Yasuda T, Susan MABH, Dokko K, Watanabe M. Binary protic ionic liquid mixtures as a proton conductor: High fuel cell reaction activity and facile proton transport. *J Phys Chem C*. 2014;118(48):27631-27639. doi:10.1021/jp506957y

10. Bayley PM, Best AS, MacFarlane DR, Forsyth M. Transport properties and phase behaviour in binary and ternary ionic liquid electrolyte systems of interest in lithium batteries. *ChemPhysChem*. 2011;12(4):823-827. doi:10.1002/cphc.201000909

11. Navia P, Troncoso J, Romaní L. Viscosities for ionic liquid binary mixtures with a common ion. *J Solution Chem*. 2008;37(5):677-688. doi:10.1007/s10953-008-9260-8

12. Song D, Chen J. Density and viscosity data for mixtures of ionic liquids with a common

anion. *J Chem Eng Data*. 2014;59(2):257-262. doi:10.1021/je400332j

13. Almeida HFD, Lopes JNC, Rebelo LPN, Coutinho JAP, Freire MG, Marrucho IM. Densities and viscosities of mixtures of two ionic liquids containing a common cation. *J Chem Eng Data*. 2016;61(8):2828-2843. doi:10.1021/acs.jced.6b00178

14. Cosby T, Kapoor U, Shah JK, Sangoro J. Mesoscale organization and dynamics in binary ionic liquid mixtures. *J Phys Chem Lett*. 2019:6274-6280. doi:10.1021/acs.jpclett.9b02478

15. Marullo S, D'Anna F, Campodonico PR, Noto R. Ionic liquid binary mixtures: How different factors contribute to determine their effect on the reactivity. *RSC Adv*. 2016;6(93):90165-90171. doi:10.1039/c6ra12836j

16. Cha S, Kim D. Change of hydrogen bonding structure in ionic liquid mixtures by anion type. *J Chem Phys*. 2018;148(19). doi:10.1063/1.5010067

17. Payal RS, Balasubramanian S. Homogenous mixing of ionic liquids: Molecular dynamics simulations. *Phys Chem Chem Phys*. 2013;15(48):21077-21083. doi:10.1039/c3cp53492h

18. Matthews RP, Villar-Garcia IJ, Weber CC, et al. A structural investigation of ionic liquid mixtures. *Phys Chem Chem Phys*. 2016;18(12):8608-8624. doi:10.1039/c6cp00156d

19. Nemoto F, Kofu M, Nagao M, et al. Neutron scattering studies on short- and long-range layer structures and related dynamics in imidazolium-based ionic liquids. *J Chem Phys*. 2018;149(5). doi:10.1063/1.5037217

20. Andanson JM, Beier MJ, Baiker A. Binary ionic liquids with a common cation: Insight into nanoscopic mixing by infrared spectroscopy. *J Phys Chem Lett*. 2011;2(23):2959-2964. doi:10.1021/jz201323a

21. Kunze M, Jeong S, Paillard E, Winter M, Passerini S. Melting behavior of pyrrolidinium-based ionic liquids and their binary mixtures. *J Phys Chem C*. 2010;114(28):12364-12369. doi:10.1021/jp103746k

22. Shimizu K, Tariq M, Rebelo LPN, Lopes JNC. Binary mixtures of ionic liquids with a common ion revisited: A molecular dynamics simulation study. *J Mol Liq*. 2010;153(1):52-56. doi:10.1016/j.molliq.2009.07.012

23. Annat G, Forsyth M, MacFarlane DR. Ionic liquid mixtures-variations in physical properties and their origins in molecular structure. *J Phys Chem B*. 2012;116(28):8251-8258. doi:10.1021/jp3012602

24. Bruce DW, Cabry CP, Lopes JNC, et al. Nanosegregation and structuring in the bulk and at the surface of ionic-liquid mixtures. *J Phys Chem B*. 2017;121(24):6002-6020. doi:10.1021/acs.jpcb.7b01654

25. Kanakubo M, Makino T, Umecky T. CO2 solubility in and physical properties for ionic liquid mixtures of 1-butyl-3-methylimidazolium acetate and 1-butyl-3-methylimidazolium bis(trifluoromethanesulfonyl)amide. *J Mol Liq*. 2016;217:112-119. doi:10.1016/j.molliq.2016.02.018

26. Xiao D, Rajian JR, Li S, Bartsch RA, Quitevis EL. Additivity in the optical Kerr effect spectra of binary ionic liquid mixtures: Implications for nanostructural organization. *J Phys Chem B*. 2006;110(33):16174-16178. doi:10.1021/jp063740o

27. Russina O, Lo Celso F, Plechkova N V., Triolo A. Emerging evidences of mesoscopic-scale complexity in neat ionic liquids and their mixtures. *J Phys Chem Lett*.

2017;8(6):1197-1204. doi:10.1021/acs.jpclett.6b02811

28. Weber CC, Brooks NJ, Castiglione F, et al. On the structural origin of free volume in 1-alkyl-3-methylimidazolium ionic liquid mixtures: A SAXS and 129Xe NMR study. *Phys Chem Chem Phys*. 2019;21(11):5999-6010. doi:10.1039/c9cp00587k

29. Docampo-Álvarez B, Gómez-González V, Méndez-Morales T, et al. The effect of alkyl chain length on the structure and thermodynamics of protic-aprotic ionic liquid mixtures: A molecular dynamics study. *Phys Chem Chem Phys*. 2018;20(15):9938-9949. doi:10.1039/c8cp00575c

30. Herrera C, Atilhan M, Aparicio S. A theoretical study on mixtures of amino acid-based ionic liquids. *Phys Chem Chem Phys*. 2018;20(15):10213-10223. doi:10.1039/c7cp08533h

31. Brooks NJ, Castiglione F, Doherty CM, et al. Linking the structures, free volumes, and properties of ionic liquid mixtures. *Chem Sci*. 2017;8(9):6359-6374. doi:10.1039/c7sc01407d

32. Lepre LF, Szala-Bilnik J, Padua AAH, Traïkia M, Ando RA, Costa Gomes MF. Tailoring the properties of acetate-based ionic liquids using the tricyanomethanide anion. *Phys Chem Chem Phys*. 2016;18(33):23285-23295. doi:10.1039/c6cp04651g

33. Hollõczki O, Macchiagodena M, Weber H, et al. Triphilic ionic-liquid mixtures: fluorinated and non-fluorinated aprotic ionic-liquid mixtures. *ChemPhysChem*. 2015;16(15):3325-3333. doi:10.1002/cphc.201500473

34. Russina O, Triolo A. New experimental evidence supporting the mesoscopic segregation model in room temperature ionic liquids. *Faraday Discuss*. 2012;154:97-109.

doi:10.1039/c1fd00073j

35. Bini R, Bortolini O, Chiappe C, Pieraccini D, Siciliano T. Development of cation/anion "interaction" scales for ionic liquids through ESI-MS measurements. *J Phys Chem B*. 2007;111(3):598-604. doi:10.1021/jp0663199

36. Nanda R, Damodaran K. A review of NMR methods used in the study of the structure and dynamics of ionic liquids. *Magn Reson Chem*. 2018;56(2):62-72. doi:10.1002/mrc.4666

37. Giernoth R. NMR spectroscopy in ionic liquids. *Top Curr Chem*. 2009;290:263-283. doi:10.1007/128

38. D'Agostino C, Mantle MD, Mullan CL, Hardacre C, Gladden LF. Diffusion, ion pairing and aggregation in 1-ethyl-3-methylimidazolium-based ionic liquids studied by 1H and 19F PFG NMR: Effect of temperature, anion and glucose dissolution. *ChemPhysChem*. 2018;19(9):1081-1088. doi:10.1002/cphc.201701354

39. Weingärtner H. Understanding ionic liquids at the molecular level: Facts, problems, and controversies. *Angew Chemie - Int Ed*. 2008;47(4):654-670. doi:10.1002/anie.200604951

40. Holbrey JD, Seddon KR. Tetrafluoroborates ; Ionic Liquids and Ionic Liquid Crystals. 1999:2133-2139.

41. Carper WR, Wahlbeck PG, Dölle A. 13C NMR relaxation rates: Separation of dipolar and chemical shift anisotropy effects. *J Phys Chem A*. 2004;108(29):6096-6099. doi:10.1021/jp031300g

42. Antony JH, Mertens D, Dölle A, Wasserscheid P, Carper WR. Molecular reorientational dynamics of the neat ionic liquid 1-butyl-3-methylimidazolium hexafluorophosphate by

measurement of 13C nuclear magnetic relaxation data. *ChemPhysChem*. 2003;4(6):588-594. doi:10.1002/cphc.200200603

43. Remsing RC, Hernandez G, Swatloski RP, Massefski WW, Rogers RD, Moyna G. Solvation of carbohydrates in N,N'-dialkylimidazolium ionic liquids: A multinuclear NMR spectroscopy study. *J Phys Chem B*. 2008;112(35):11071-11078. doi:10.1021/jp8042895

44. Strate A, Neumann J, Overbeck V, et al. Rotational and translational dynamics and their relation to hydrogen bond lifetimes in an ionic liquid by means of NMR relaxation time experiments and molecular dynamics simulation. *J Chem Phys*. 2018;148(19). doi:10.1063/1.5011804

45. Nakamura K, Shikata T. Systematic dielectric and NMR study of the ionic liquid 1-alkyl-3-methyl imidazolium. *ChemPhysChem*. 2010;11(1):285-294. doi:10.1002/cphc.200900642

46. Hayamizu K, Tsuzuki S, Seki S, Umebayashi Y. Nuclear magnetic resonance studies on the rotational and translational motions of ionic liquids composed of 1-ethyl-3-methylimidazolium cation and bis(trifluoromethanesulfonyl)amide and bis(fluorosulfonyl)amide anions and their binary systems including li. *J Chem Phys*. 2011;135(8). doi:10.1063/1.3625923

47. Imanari M, Fujii K, Mukai T, Mizushima N, Seki H, Nishikawa K. Anion and cation dynamics of sulfonylamide-based ionic liquids and the solid-liquid transitions. *Phys Chem Chem Phys*. 2015;17(14):8750-8757. doi:10.1039/c5cp00302d

48. Shimizu Y, Wachi Y, Fujii K, Imanari M, Nishikawa K. NMR study on ion dynamics and phase behavior of a piperidinium-based room-temperature ionic liquid: 1-butyl-1-methylpiperidinium bis(fluorosulfonyl)amide. *J Phys Chem B*. 2016;120(25):5710-5719. doi:10.1021/acs.jpcb.6b04095

49. Allen JJ, Bowser SR, Damodaran K. Molecular interactions in the ionic liquid emim acetate and water binary mixtures probed via NMR spin relaxation and exchange spectroscopy. *Phys Chem Chem Phys*. 2014;16(17):8078-8085. doi:10.1039/c3cp55384a

50. Alam TM, Dreyer DR, Bielwaski CW, Ruoff RS. Measuring molecular dynamics and activation energies for quaternary acyclic ammonium and cyclic pyrrolidinium ionic liquids using 14N NMR spectroscopy. *J Phys Chem A*. 2011;115(17):4307-4316. doi:10.1021/jp200630k

51. Bystrov SS, Matveev V V., Chernyshev YS, Balevičius V, Chizhik VI. Molecular mobility in a set of imidazolium-based ionic liquids [bmim]+A- by the NMR-relaxation method. *J Phys Chem B*. 2019;123(10):2362-2372. doi:10.1021/acs.jpcb.8b11250

52. Rumble CA, Kaintz A, Yadav SK, et al. Rotational dynamics in ionic liquids from NMR relaxation experiments and simulations: Benzene and 1-ethyl-3-methylimidazolium. *J Phys Chem B*. 2016;120(35):9450-9467. doi:10.1021/acs.jpcb.6b06715

53. Allen JJ, Schneider Y, Kail BW, Luebke DR, Nulwala H, Damodaran K. Nuclear spin relaxation and molecular interactions of a novel triazolium-based ionic liquid. *J Phys Chem B*. 2013;117(14):3877-3883. doi:10.1021/jp401188g

54. Endo T, Murata H, Imanari M, et al. A comparative study of the rotational dynamics of PF

6- anions in the crystals and liquid states of 1-butyl-3- methylimidazolium hexafluorophosphate: Results from 31 P NMR spectroscopy. *J Phys Chem B*. 2013;117(1):326-332. doi:10.1021/jp310947c

55. Klimavicius V, Bacevicius V, Gdaniec Z, Balevicius V. Pulsed- field gradient 1H NMR study of diffusion and self-aggregation of long-chain imidazolium-based ionic liquids. *J Mol Liq*. 2015;210:223-226.

56. Gordon PG, Brouwer DH, Ripmeester JA. Probing the local structure of pure ionic liquid salts with solid- and liquid-state NMR. *ChemPhysChem*. 2010;11(1):260-268. doi:10.1002/cphc.200900624

57. Klimavicius V, Gdaniec Z, Balevicius V. Very short NMR relaxation times of anions in ionic liquids: New pulse sequence to eliminate the acoustic ringing. *Spectrochim Acta - Part A Mol Biomol Spectrosc*. 2014;132:879-883. doi:10.1016/j.saa.2014.04.140

58. Endo T, Murata H, Imanari M, Mizushima N, Seki H, Nishikawa K. NMR study of cation dynamics in three crystalline states of 1-butyl-3-methylimidazolium hexafluorophosphate exhibiting crystal polymorphism. *J Phys Chem B*. 2012;116(12):3780-3788. doi:10.1021/jp300636s

59. Hayamizu K, Tsuzuki S, Seki S, Fujii K, Suenaga M, Umebayashi Y. Studies on the translational and rotational motions of ionic liquids composed of N -methyl- N -propyl-pyrrolidinium (P13) cation and bis(trifluoromethanesulfonyl)amide and bis(fluorosulfonyl)amide anions and their binary systems including lithium salts. *J Chem Phys*. 2010;133(19). doi:10.1063/1.3505307

60. Hayamizu K, Tsuzuki S, Seki S, Umebayashi Y. Multinuclear NMR studies on translational and rotational motion for two ionic liquids composed of BF4 anion. *J Phys Chem B.* 2012;116(36):11284-11291. doi:10.1021/jp306146s

61. Alam TM, Dreyer DR, Bielawski CW, Ruoff RS. Combined measurement of translational and rotational diffusion in quaternary acyclic ammonium and cyclic pyrrolidinium ionic liquids. *J Phys Chem B.* 2013;117(6):1967-1977. doi:10.1021/jp3111953

62. Martinelli A, Maréchal M, Östlund Å, Cambedouzou J. Insights into the interplay between molecular structure and diffusional motion in 1-alkyl-3-methylimidazolium ionic liquids: A combined PFG NMR and X-ray scattering study. *Phys Chem Chem Phys*. 2013;15(15):5510-5517. doi:10.1039/c3cp00097d

63. Nanda R. Thermal dynamics of lithium salt mixtures of ionic liquid in water by PGSE NMR spectroscopy. *RSC Adv*. 2016;6(43):36394-36406. doi:10.1039/c6ra00891g

64. Noda A, Hayamizu K, Watanabe M. Pulsed-gradient spin-echo 1H and 19F NMR ionic diffusion coefficient, viscosity, and ionic conductivity of non-chloroaluminate room-temperature ionic liquids. *J Phys Chem B.* 2001;105(20):4603-4610. doi:10.1021/jp004132q

65. Sangoro J, Iacob C, Serghei A, et al. Electrical conductivity and translational diffusion in the 1-butyl-3-methylimidazolium tetrafluoroborate ionic liquid. *J Chem Phys*. 2008;128(21). doi:10.1063/1.2921796

66. Chiappe C, Sanzone A, Mendola D, et al. Pyrazolium- versus imidazolium-based ionic liquids: Structure, dynamics and physicochemical properties. *J Phys Chem B.*

2013;117(2):668-676. doi:10.1021/jp3107793

67. Casalegno M, Raos G, Appetecchi GB, Passerini S, Castiglione F, Mele A. From nanoscale to microscale: crossover in the diffusion dynamics within two pyrrolidinium-based ionic liquids. *J Phys Chem Lett*. 2017;8(20):5196-5202. doi:10.1021/acs.jpclett.7b02431

68. Annat G, MacFarlane DR, Forsyth M. Transport properties in ionic liquids and ionic liquid mixtures: The challenges of NMR pulsed field gradient diffusion measurements. *J Phys Chem B*. 2007;111(30):9018-9024. doi:10.1021/jp072737h

69. Castiglione F, Moreno M, Raos G, et al. Structural organization and transport properties of novel pyrrolidinium-based ionic liquids with perfluoroalkyl sulfonylimide anions. *J Phys Chem B*. 2009;113(31):10750-10759. doi:10.1021/jp811434e

70. Judeinstein P, Iojoiu C, Sanchez JY, Ancian B. Proton conducting ionic liquid organization as probed by NMR: Self-diffusion coefficients and heteronuclear correlations. *J Phys Chem B*. 2008;112(12):3680-3683. doi:10.1021/jp711298g

71. Mantz RA, Trulove PC, Carlin RT, Osteryoung RA. ROESY NMR of basic ambient-temperature chloroaluminate ionic liquids. *Inorg Chem*. 1995;34(14):3846-3847. doi:10.1021/ic00118a042

72. Mele A, Romanò G, Giannone M, et al. The local structure of ionic liquids: Cation-cation NOE interactions and internuclear distances in neat [BMIM][BF4] and [BDMIM]-[BF 4]. *Angew Chemie - Int Ed*. 2006;45(7):1123-1126. doi:10.1002/anie.200503745

73. Lingscheid Y, Arenz S, Giernoth R. Heteronuclear NOE spectroscopy of ionic liquids.

ChemPhysChem. 2012;13(1):261-266. doi:10.1002/cphc.201100622

74. Dupont J, Suarez PAZ, De Souza RF, Burrow RA, Kintzinger JP. C-H-π interactions in 1-n-butyl-3-methylimidazolium tetraphenylborate molten salt: Solid and solution structures. *Chem - A Eur J*. 2000;6(13):2377-2381. doi:10.1002/1521-3765(20000703)6:13<2377::AID-CHEM2377>3.0.CO;2-L

75. Gutel T, Santini CC, Pádua AAH, et al. Interaction between the π-system of toluene and the imidazolium ring of ionic liquids: A combined NMR and Molecular Simulation Study. *J Phys Chem B*. 2009;113(1):170-177. doi:10.1021/jp805573t

76. Gabl S, Steinhauser O, Weingärtner H. From short-range to long-range intermolecular NOEs in ionic liquids: Frequency does matter. *Angew Chemie - Int Ed*. 2013;52(35):9242-9246. doi:10.1002/anie.201302712

77. Castiglione F, Appetecchi GB, Passerini S, Panzeri W, Indelicato S, Mele A. Multiple points of view of heteronuclear NOE: Long range vs short range contacts in pyrrolidinium based ionic liquids in the presence of Li salts. *J Mol Liq*. 2015;210:215-222. doi:10.1016/j.molliq.2015.05.036

78. Martin PA, Chen F, Forsyth M, Deschamps M, O'Dell LA. Correlating intermolecular cross-relaxation rates with distances and coordination numbers in ionic liquids. *J Phys Chem Lett*. 2018;9(24):7072-7078. doi:10.1021/acs.jpclett.8b03021

79. Bax A, Grzesiek S. Roesy. *Encycl Magn Reson*. 2007:1-10. doi:10.1002/9780470034590.emrstm0473

80. Martin PA, Salager E, Forsyth M, O'Dell LA, Deschamps M. On the measurement of

intermolecular heteronuclear cross relaxation rates in ionic liquids. *Phys Chem Chem Phys*. 2018;20(19):13357-13364. doi:10.1039/c8cp00911b

81. Cesare Marincola F, Piras C, Russina O, Gontrani L, Saba G, Lai A. NMR investigation of imidazolium-based ionic liquids and their aqueous mixtures. *ChemPhysChem*. 2012;13(5):1339-1346. doi:10.1002/cphc.201100810

82. Khatun S, Castner EW. Ionic liquid-solute interactions studied by 2D NOE NMR spectroscopy. *J Phys Chem B*. 2015;119(29):9225-9235. doi:10.1021/jp509861g

83. Lee HY, Shirota H, Castner EW. Differences in ion interactions for isoelectronic ionic liquid homologs. *J Phys Chem Lett*. 2013;4(9):1477-1483. doi:10.1021/jz400465x

TOC